



## Active Curved Polymers Form Vortex Patterns on Membranes

Jonas Denk, Lorenz Huber, Emanuel Reithmann, and Erwin Frey\*

*Arnold Sommerfeld Center for Theoretical Physics (ASC) and Center for NanoScience (CeNS), Department of Physics, Ludwig-Maximilians-Universität München, Theresienstrasse 37, D-80333 München, Germany*

(Received 16 June 2015; revised manuscript received 9 December 2015; published 25 April 2016)

Recent *in vitro* experiments with FtsZ polymers show self-organization into different dynamic patterns, including structures reminiscent of the bacterial Z ring. We model FtsZ polymers as active particles moving along chiral, circular paths by Brownian dynamics simulations and a Boltzmann approach. Our two conceptually different methods point to a generic phase behavior. At intermediate particle densities, we find self-organization into vortex structures including closed rings. Moreover, we show that the dynamics at the onset of pattern formation is described by a generalized complex Ginzburg-Landau equation.

DOI: 10.1103/PhysRevLett.116.178301

Intracellular structuring is often facilitated by the active dynamics of cytoskeletal constituents. The origin of these driven dynamics and their impact on pattern formation has been extensively studied using artificial motility assays of cytoskeletal filaments [1–4]. Another intriguing example of self-organization due to driven filaments was reported recently by Loose and Mitchison [5]. *In vitro*, the bacterial protein FtsZ forms membrane-bound, intrinsically curved polymers. These seem to exhibit treadmilling dynamics (consuming guanosine triphosphate) and, as a result, move clockwise on the membrane. Depending on the protein density, polymers cluster into dynamic structures such as rotating rings or jammed bundles, despite the absence of attractive interactions [6]. These ring structures are of particular interest, since, *in vivo*, FtsZ builds the contractile Z ring which drives cell division in a yet unknown way [7–9]. But also in the *in vitro* experiments, the pattern-forming mechanism remains unclear even on a qualitative level.

Motivated by these experimental findings, we have studied pattern formation in a class of active systems, where particles move on circular tracks and interact only via steric repulsion. To assess the dynamics of this class, we consider two conceptually different models: First, we emulate active particles as elastic polymers with fixed intrinsic curvature that move with a constant tangential velocity [Fig. 1(a)] and perform Brownian dynamics simulations. Second, we employ a kinetic Boltzmann approach, where pointlike particles move on circular paths and undergo diffusion and binary collisions (with polar symmetry) according to a simplified collision rule [Fig. 1(b)]. As a result, we identify different phases of collective behavior as a function of density and noise level. With both approaches, we find flocking into vortex patterns in

the regime of intermediate density and noise strength. Our simulations for extended particles predict the formation of closed ring structures reminiscent of those found in Ref. [5], even in the absence of any attractive interactions. In the mesoscopic limit, our analysis yields that, close to the onset of vortex formation, the dynamics at the onset of ordering is characterized by a novel generalization of the complex Ginzburg-Landau equation.

In our Brownian dynamics simulations, we consider a system of  $M$  curved polymers of the same chirality embedded in a two-dimensional membrane of area  $A$  with periodic boundary conditions. Each polymer is described as an inextensible wormlike chain [10,11] of length  $L$ , persistence length  $\ell_p$ , and intrinsic curvature  $\kappa_0$ . For a given polymer conformation  $\mathbf{r}(s)$ , parameterized in terms of arc length  $s$ , the overall bending energy is given by  $E_{\text{bend}} = \frac{1}{2} \ell_p k_B T \int_0^L ds [\kappa(s) - \kappa_0]^2$ , where  $\kappa(s) = |\partial_s^2 \mathbf{r}(s)|$  denotes the local curvature. Excluded volume interaction is implemented by a repulsive truncated Lennard-Jones potential. To assure motion of the filament contour on a circular track (apart from noise), polymers are propelled with a tangential velocity  $\mathbf{v}_0(s) = v_0 \partial_s \mathbf{r}(s)$ . This accounts for the effective motion of treadmilling in a simplified way [12].

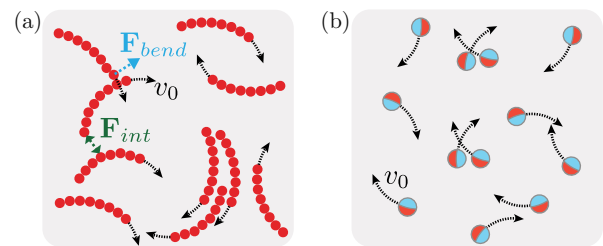


FIG. 1. Systems of active particles, which are driven on chiral, circular tracks with speed  $v_0$ : (a) *Microscopic view*: Extended, elastic polymers with intrinsic curvature, where noise and steric interaction trigger bending of filaments. (b) *Mesoscopic view*: Pointlike particles that undergo diffusion as well as binary collisions.

Published by the American Physical Society under the terms of the *Creative Commons Attribution 3.0 License*. Further distribution of this work must maintain attribution to the author(s) and the published article's title, journal citation, and DOI.

Note that, for this choice, the area explored by a circling polymer is minimal. In the free draining limit, the dynamics of the polymer system is then determined by a set of coupled Langevin equations for the contours  $\mathbf{r}^{(m)}(t, s)$  of each polymer  $m = 1, 2, \dots, M$ :  $\zeta(\partial_t \mathbf{r}^{(m)} - \mathbf{v}_0^{(m)}) = -\delta E[\{\mathbf{r}^{(n)}\}] / \delta \mathbf{r}^{(m)} + \boldsymbol{\eta}^{(m)}$ , balancing viscous friction with elastic and repulsive forces generated by the total energy  $E$  and Langevin noise  $\boldsymbol{\eta}$  with zero mean and  $\langle \boldsymbol{\eta}(t, s) \cdot \boldsymbol{\eta}(t', s') \rangle = 4k_B T \zeta \delta(t - t') \delta(s - s')$ . To numerically solve the polymer dynamics, we employ a bead-spring representation of the polymers [12,17,18]. For most simulations, we adapted length scales close to those observed in Refs. [5,8]:  $\kappa_0^{-1} = 0.5 \mu\text{m}$ ,  $L = 0.9 \mu\text{m}$ , and  $\ell_p = 10 \mu\text{m}$ . The relevant dimensionless parameters that characterize the system are the reduced noise  $\sigma$  and density  $\rho$ . Here,  $\sigma := k_B T \ell_p / (\zeta v_0 L^2)$  relates thermal forces at length scale  $\ell_p$  with friction forces, and  $\rho := (R_0/b)^2$  denotes the squared ratio of the radius of curvature  $R_0 = \kappa_0^{-1}$  to the mean polymer distance  $b = \sqrt{A/M}$ .

For dilute systems  $\rho \ll 1$ , our simulations show that each polymer is propelled on a circular path and collisions between polymers are infrequent; see Fig. 2(a) and Movie 1 in Supplemental Material [12]. The positions of the polymers' centers of curvature (CC)  $\mathbf{r}_{\text{CC}}^{(m)}$  are uncorrelated as in a gas, and we refer to this state as a *disordered state*. On increasing  $\rho$ , we observe that a significant fraction of filaments begin to collide and collect into localized vortex structures (*vortex state*). These ringlike structures are

highly dynamic. They assemble and persist for several rotations, during which their centers of mass remain relatively static; see Fig. 2(b) and Movie 2 [12]. Despite our simplified kinetic assumption, the overall phenomenology resembles the FtsZ patterns observed by Loose and Mitchison [5], including vortex assembly, disassembly, and localization. In the dense regime  $\rho \gtrsim 1$ , where each polymer is likely to collide, these vortices are unstable. Instead, the polymers cluster and form jammed “trains” that travel through the system in an irregular fashion; see Fig. 2(c) and Movie 3 [12].

In order to quantitatively distinguish between the various observed patterns and organize them into a “phase diagram,” we consider the pair correlation function  $g(d_{\text{CC}})$  [19,20] of distances  $d_{\text{CC}} = |\mathbf{r}_{\text{CC}}^{(m)} - \mathbf{r}_{\text{CC}}^{(n)}|$  between the centers of curvature [Fig. 2(d)]. We regard a system as disordered if  $g(d_{\text{CC}})$  exhibits a minimum at a distance  $d_{\text{CC}}^{\text{min}}$  equal to the diameter of a free circular path,  $d_{\text{CC}}^{\text{min}} \approx 2R_0$ . This is distinct from vortex states, where  $d_{\text{CC}}^{\text{min}}$ , defining an effective vortex diameter, is larger than  $2R_0$ . Finally, for train states,  $g(d_{\text{CC}})$  does not exhibit a local minimum, indicating the absence of an isolated vortex structure; for more details, see Supplemental Material [12]. The ensuing phase diagram is shown in Fig. 2(d). As in other active systems [21–28], pattern formation is favored by increasing density and decreasing noise strength. Jammed states prevail only when the density is high and the noise level low. Note also that the structure of the phase diagram depends on the ratio of filament length  $L$  to radius of curvature  $R_0$ . Polymers with an arc angle close to  $\kappa_0 L = 2\pi$  (closed circles) retain a single-circle structure and do not form any collective structures upon increasing  $\rho$  (Movie 4 [12]). Conversely, reducing  $\kappa_0 L$  suppresses the formation of closed ring structures, due to inefficient alignment of short polymers. Instead, these polymers cluster into flocks which move on approximately circular paths (Movie 5 [12]). Hence, we conclude that the range of arc angles of FtsZ polymers,  $\kappa_0 L \approx 0.6\pi$ , observed *in vitro* [5], facilitates the formation of closed polymer rings particularly well [Fig. 2(b)]. In summary, closed polymer rings require explicit curvature and filament lengths larger than a certain threshold value. For other interactions than local, steric repulsion ring structures may also emerge [1,3,29]; straight, rotating rods may form vortex arrays but not closed rings [30].

We complement the Brownian dynamics simulations of active particles that are propelled on circular tracks by considering the mesoscopic limit of a vanishing particle extension. To this end, we have employed a kinetic Boltzmann approach [24,31–36] to determine the collective behavior and the corresponding phase transitions in this limit, irrespective of the microscopic details of the constituent particles. In detail, we simplified the active system to one consisting of spherical particles (of diameter  $d$ ) moving clockwise with constant speed  $v_0$  on circular orbits of radius  $R_0$ . This accounts for both self-propulsion and

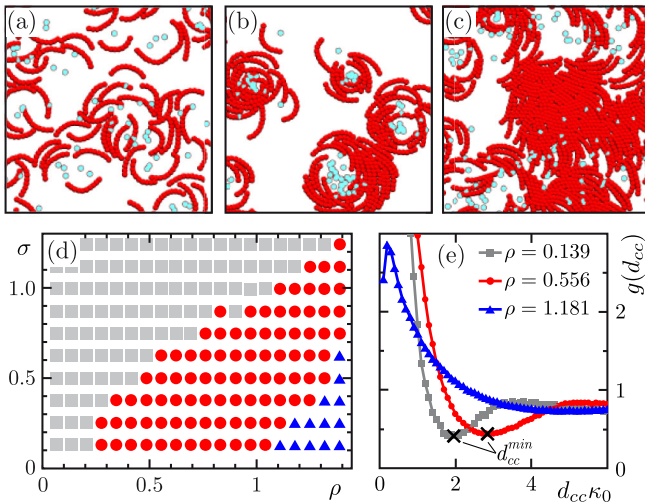


FIG. 2. System snapshots are provided to depict (a) disorder ( $\rho = 0.556$ ,  $\sigma = 0.987$ ), (b) vortices ( $\rho = 0.556$ ,  $\sigma = 0.247$ ), and (c) trains ( $\rho = 1.389$ ,  $\sigma = 0.247$ ). Curvature centers  $\mathbf{r}_{\text{CC}}^{(m)}$  are depicted by light blue dots. (d) Phase portrait for varying density  $\rho$  and noise  $\sigma$ : disorder states (gray rectangles), vortex states (red circles), and train states (blue triangles). (e) Pair correlation function  $g(d_{\text{CC}})$  for the three different states with  $\sigma = 0.247$  and  $\rho$  indicated in the graph.

spontaneous curvature but neglects the finite extension of the polymers as compared to our Brownian dynamics simulations.

We further assume that a particle's orientation is altered by "self-diffusion" as well as by local binary collisions. In self-diffusion, a particle's instantaneous orientation  $\theta$  changes at rate  $\lambda$  into  $\theta + \eta$ , where we assume  $\eta$  to be Gaussian distributed with standard deviation  $\sigma$ . As in other particle-based active systems [32,34,37], binary collisions are modeled by a polar alignment rule where the orientations of the collision partners align along their average angle plus a Gaussian-distributed fluctuation; for simplicity, we take the same width  $\sigma$  as for self-diffusion.

The kinetic Boltzmann equation [24,31–36] for the one-particle distribution function  $f(\mathbf{r}, \theta, t)$  then reads

$$\partial_t f + v_0[\mathbf{e}_\theta \cdot \partial_{\mathbf{r}} + \kappa_0 \partial_\theta] f = \mathcal{I}_d[f] + \mathcal{I}_c[f, f]. \quad (1)$$

It describes the dynamics of the density of particles in phase-space element  $d\mathbf{r}d\theta$  which is being convected due to particle self-propulsion and which undergoes rotational diffusion and binary particle collisions, as given by the collision integrals  $\mathcal{I}_d[f]$  and  $\mathcal{I}_c[f, f]$ , respectively; for explicit expressions, please see Supplemental Material [12]. Note here the critical difference from field theories for straight-moving particles [32,38–40]; there is an additional angular derivative in the convection term, which reflects the fact that the particles are moving on circular orbits. In the following, we rescale the time, space, and density such that  $v_0 = \lambda = d = 1$ . Then, the only remaining free parameters are the noise amplitude  $\sigma$ ,  $\kappa_0$ , and the mean particle density  $\bar{\rho} = A^{-1} \int_A d\mathbf{r} \int_{-\pi}^{\pi} d\theta f(\mathbf{r}, \theta, t)$  measured in units of  $\lambda/(dv_0)$ , i.e., the number of particles found within the area traversed by a particle between successive self-diffusion events.

To identify possible solutions of the Boltzmann equation and analyze their stability, we performed a spectral analysis. Upon expanding the one-particle distribution function in terms of Fourier modes of the angular variable,  $f_k(\mathbf{r}, t) = \int_{-\pi}^{\pi} d\theta e^{i\theta k} f(\mathbf{r}, \theta, t)$ , one obtains

$$\begin{aligned} \partial_t f_k + \frac{v_0}{2} [\partial_x (f_{k+1} + f_{k-1}) - i\partial_y (f_{k+1} - f_{k-1})] - ikv_0\kappa_0 f_k \\ = -\lambda(1 - e^{-(k\sigma)^2/2})f_k + \sum_{n=-\infty}^{\infty} \mathcal{I}_{n,k} f_n f_{k-n}, \end{aligned} \quad (2)$$

where explicit expressions for the collision kernels  $\mathcal{I}_{n,k}(\sigma)$  are given in Supplemental Material [12]. For  $k = 0$ , Eq. (2) yields the continuity equation  $\partial_t \rho = -\nabla \cdot \mathbf{j}$  for the local density  $\rho(\mathbf{r}, t) := f_0(\mathbf{r}, t)$  with the particle current given by  $\mathbf{j}(\mathbf{r}, t) = v_0(\text{Re}f_1, \text{Im}f_1)^T$ . In general, Eq. (2) constitutes an infinite hierarchy of equations coupling lower- with higher-order Fourier modes.

A linear stability analysis of Eq. (2) enables further progress. Since  $\mathcal{I}_{n,0} = 0$  for all  $n$ , a state with spatially

homogeneous density  $\bar{\rho} = f_0$  and all higher Fourier modes vanishing is a stationary solution to Eq. (2) (disordered state). To linear order, the dynamics of small perturbations  $\delta f_k$  with respect to this uniform state is given by  $\partial_t \delta f_k = \mu_k(\bar{\rho}, \sigma) \delta f_k$ , where  $\mu_k(\bar{\rho}, \sigma) = (\mathcal{I}_{0,k} + \mathcal{I}_{k,k})\bar{\rho} - \lambda(1 - e^{-(k\sigma)^2/2})$ . For a polar collision rule, as considered here, only  $\mu_1$  can become positive, defining a critical density  $\rho_c(\sigma)$  at  $\mu_1(\rho_c, \sigma) := 0$  [Fig. 3(a)]. Above the threshold ( $\bar{\rho} > \rho_c$ ), the spatially homogeneous state is unstable, the particle current grows exponentially, and collective motion may emerge.

In close proximity to the critical density  $\rho_c(\sigma)$ , a weakly nonlinear analysis yields further insights into the dynamics of the system and the ensuing steady states. Here we follow Ref. [31] and assume small currents  $f_1 \ll 1$  at the onset. Then, balancing of the terms in the continuity equation, the equation for  $f_1$ , and terms involving  $f_1$  in the equation for  $f_2$  implies the scaling  $\rho - \bar{\rho} \sim f_1$ ,  $f_2 \sim f_1^2$  as well as weak spatial and temporal variations  $\partial_{x/y} \sim f_1$ ,  $\partial_t \sim f_1$ . To include the lowest-order damping term in  $f_1$ , we retain terms up to cubic order in  $f_1$ . This yields the following hydrodynamic equation for the complex particle current  $v_0 f_1(\mathbf{r}, t) = j_x(\mathbf{r}, t) + ij_y(\mathbf{r}, t)$ :

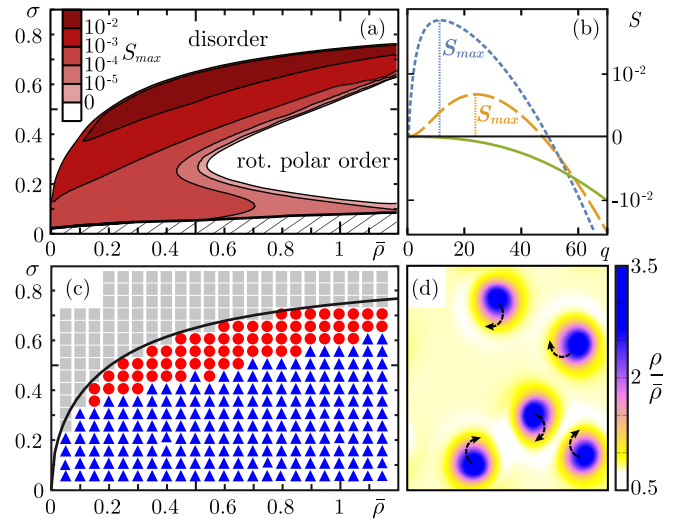


FIG. 3. (a) Stability of homogeneous solutions of Eq. (2) as a function of  $\sigma$  and  $\bar{\rho}$  in units of  $\lambda/(dv_0)$ . White and red areas denote regions where finite wavelength perturbations of the homogeneous solutions are stable and unstable, respectively. The color code denotes the value of the maximal growth rate  $S_{\max}$ . (b) Dispersion relation of  $S(q)$  ( $q$  in units of  $2\pi/\sqrt{A}$ ) for  $\bar{\rho} = 0.8$  and  $\sigma = 0.7$  (short-dashed line),  $\sigma = 0.6$  (long-dashed line), and  $\sigma = 0.4$  (solid line). Vertical lines indicate  $S_{\max}$ . (c) Phase diagram for density  $\bar{\rho}$  and  $\sigma$  displaying phases of homogeneous disorder (gray rectangles), swirls (red circles), and homogeneous order (blue triangles). The solid line marks the analytic solution of  $\rho_c(\sigma)$ . An overlay of (a) and (c) can be found in Supplemental Material [12]. (d) Snapshot of swirl patterns ( $\bar{\rho} = 0.8$ ,  $\sigma = 0.7$ ). All swirls are moving clockwise on circular paths.

$$\begin{aligned} \partial_t f_1(\mathbf{r}, t) = & [\alpha(\rho - \rho_c) + iv_0\kappa_0]f_1 - \xi|f_1|^2f_1 - \frac{v_0}{2}\nabla\rho \\ & - \beta f_1^*\nabla f_1 - \gamma f_1\nabla^* f_1 + \nu\nabla^*\nabla f_1, \end{aligned} \quad (3)$$

where  $\nabla := \partial_x + i\partial_y$ . While this equation shows similar functional dependencies on local density and current as found in systems without [41] and with straight propulsion [32], the coefficients  $\alpha$ ,  $\xi$ ,  $\nu$ ,  $\gamma$ , and  $\beta$  are now *complex valued* (for explicit expressions, please see Supplemental Material [12]). This can be traced back to the angular convection term in Eq. (1) or, equivalently, to the corresponding phase-shift term in Eq. (2). As a consequence, the field theory of active systems with particles moving on circular orbits with defined chirality is generically given by a complex Ginzburg-Landau (GL) equation with convective spatial coupling as well as density-current coupling. This constitutes a highly interesting generalization of the standard (diffusive) complex GL equations [42,43] and is qualitatively different from real GL-type equations that were previously applied in the context of self-propelled particles [31]. Above the threshold,  $\bar{\rho} > \rho_c(\sigma)$ , the active chiral hydrodynamics described by the generalized GL equation (3) exhibits a uniform oscillatory solution with  $f_1 = F_1 e^{i\Omega_0 t}$ , i.e., a state in which particles move on a circular (chiral) path with an angular velocity  $\Omega_0 = v_0\kappa_0 - \alpha(\bar{\rho} - \rho_c)\text{Im}[\xi]/\text{Re}[\xi]$ ; the amplitude  $F_1 = \{\alpha(\bar{\rho} - \rho_c)/\text{Re}[\xi]\}^{1/2}$  gives the particle density. However, a linear stability analysis of Eq. (3) shows that for densities slightly larger than  $\rho_c$  this oscillatory solution is linearly unstable against finite wavelength perturbations in the current and density fields. Preliminary numerical solutions of the generalized GL equation [Eq. (3)] take the form of rotating spots of high density that appear to show turbulent dynamics [12,44]. This is qualitatively distinct from the high-density bands found for straight-moving particles [23,45] and the vortex field of a fluid coupled to torque dipoles [46,47].

Far above the threshold, closure relations such as those discussed above [31] may become invalid and with them the ensuing hydrodynamic equations. Therefore, we proceed with the full spectral analysis of the Boltzmann equation [Eq. (2)] as detailed in Supplemental Material [12]. First, we numerically calculate the spatially homogeneous solutions for all angular Fourier modes  $f_k$  below some cutoff wave vector  $k_{\max}$ . For given values of  $\bar{\rho}$  and  $\sigma$  and a desired accuracy  $\varepsilon$  of this mode truncation scheme, the cutoff is chosen such that  $|f_{k_{\max}+1}| < \varepsilon$ . We find that for  $\bar{\rho} < \rho_c(\sigma)$  a spatially homogeneous state where all modes but  $f_0$  vanish is the only stable state. In contrast, above the threshold [ $\bar{\rho} > \rho_c(\sigma)$ ], there is a second solution for which  $|f_1| > 0$ . It corresponds to a polar ordered state whose orientation is changing periodically in time with frequency  $v_0\kappa_0$ . For moderate  $\bar{\rho} - \rho_c$ , the amplitude quantitatively agrees with the result from the generalized GL equation; see Supplemental Material [12]. In a second step, we

consider wavelike perturbations,  $\delta f_k(\mathbf{q})$  with wave vector  $\mathbf{q}$ , of the spatially homogeneous oscillatory solution in a corotating frame. The largest real part of all eigenvalues of the corresponding linearized system for  $\delta f_k$  then yields the linear growth rate  $S(q)$  [Fig. 3(b)]. In accordance with the linear stability analysis of Eq. (3), we find that for densities slightly larger than  $\rho_c$  a spatially homogeneous solution is unstable against finite wavelength perturbations. The dispersion relation  $S(q)$  exhibits a band of unstable modes, with the maximal growth rate  $S_{\max}$  decreasing as one moves away from the threshold  $\rho_c$  [Figs. 3(a) and 3(b)]. Actually, there is lobelike regime in parameter space where  $S(q) < 0$  [Fig. 3(a)], and hence a homogeneously polar ordered state with rotating direction is stable. We emphasize here that our stability portrait [Fig. 3(a)] is independent of  $\kappa_0$  and hence equally valid for systems of straight-moving particles. For our two approaches [Figs. 2(d) and 3(a)], the onset to order is governed by a similar trend [12], common for active systems [28,48]: Disorder prevails for low density or high noise, and order is promoted for high density or low noise.

To determine the spatiotemporal dynamics in the regime where neither a spatially homogeneous state nor a homogeneously polar ordered state are stable, we resort to a modified version of the SNAKE algorithm [34] to numerically solve Eq. (1). It accurately reproduces the threshold value  $\rho_c(\sigma)$  at which the spatially homogeneous state becomes unstable [Fig. 3(c)]. Above the threshold ( $\bar{\rho} > \rho_c$ ), we find that local density fluctuations quickly grow and evolve into stable swirls, i.e., disklike flocks of high density and polar order moving on circular paths; see Fig. 3(d) and Movie 6 in Supplemental Material [12]. The radius of such a path is approximately given by  $R_0$ . These swirl patterns closely resemble the swirling flocks observed in the Brownian dynamics simulations for short polymer arc angles (Movie 5 [12]), as well as our preliminary numerical solutions of the generalized GL equation [Eq. (3)] [12,44]. Moreover, in accordance with the spectral analysis, we find a second threshold density, above which the system settles into a homogeneously polar ordered state with a periodically changing orientation (Movie 7 [12]). The amplitude and frequency of the polar order agree with the numerical results of the spectral analysis to high accuracy [12], while the numerically determined phase boundaries differ. The SNAKE algorithm produces stable swirl patterns only in a parameter regime where our linear stability analysis yields significant growth rates. This is mainly due to spurious noise caused by the discretization of the angular variable, which tends to suppress inhomogeneities in the regime of small growth rates. Furthermore, the finite system size constricts the band of possible modes and allows only for patterns of sufficiently short length scales.

For active systems of circling particles that interact via steric repulsion, our microscopic and mesoscopic treatments strongly suggest that a phase of collective vortex structures is a generic feature. Within this class, our work

shows that extended polymers which as a whole follow circular tracks can form closed rings. Concerning our motivation of circling FtsZ, further research is needed to elucidate the dynamics of treadmilling; yet our minimal kinetic assumption suggests that varying the particle density alone suffices to regulate the patterns as observed by Loose and Mitchison [5]. Compared to systems of straight-moving particles, we find qualitatively new phenomena [12,44]. For those systems, it was already reported that (globally achiral) vortices can occur due to collisions of particles of asymmetric shape [49] or due to memory in orientation [3,50]. Some of our findings, like the polymer length dependence of patterns and the possible emergence of active turbulence [51,52], pose interesting questions for future work. Our analysis yields a mapping of the emergent dynamics onto a generalized Ginzburg-Landau equation, providing a connection between active matter and nonlinear oscillators [44].

We thank F. Thüroff, L. Reese, and J. Knebel for helpful discussions. This research was supported by the German Excellence Initiative via the program “NanoSystems Initiative Munich” (NIM) and the graduate school “Quantitative Biosciences Munich” (QBM), and the Deutsche Forschungsgemeinschaft (DFG) via project B02 within the Collaborative Research Center (SFB 863) “Forces in Biomolecular Systems.”

J. D. and L. H. contributed equally to this work.

\*frey@lmu.de

- [1] V. Schaller, C. A. Weber, B. Hammerich, E. Frey, and A. R. Bausch, *Proc. Natl. Acad. Sci. U.S.A.* **108**, 19183 (2011).
- [2] V. Schaller, C. A. Weber, C. Semmrich, E. Frey, and A. R. Bausch, *Nature (London)* **467**, 73 (2010).
- [3] Y. Sumino, K. H. Nagai, Y. Shitaka, D. Tanaka, K. Yoshikawa, H. Chaté, and K. Oiwa, *Nature (London)* **483**, 448 (2012).
- [4] R. Suzuki, C. A. Weber, E. Frey, and A. R. Bausch, *Nat. Phys.* **11**, 839 (2015).
- [5] M. Loose and T. J. Mitchison, *Nat. Cell Biol.* **16**, 38 (2013).
- [6] E. L. Meier and E. D. Goley, *Curr. Opin. Cell Biol.* **26**, 19 (2014).
- [7] M. Ingerson-Mahar and Z. Gitai, *FEMS Microbiol. Rev.* **36**, 256 (2012).
- [8] H. P. Erickson, D. E. Anderson, and M. Osawa, *Microbiol. Mol. Biol. Rev.* **74**, 504 (2010).
- [9] P. Szwedziak, Q. Wang, T. A. M. Bharat, M. Tsim, and J. Löwe, *eLife* **3**, e04601 (2014).
- [10] O. Kratky and G. Porod, *Recl. Trav. Chim. Pays-Bas* **68**, 1106 (1949).
- [11] N. Saitô, K. Takahashi, and Y. Yunoki, *J. Phys. Soc. Jpn.* **22**, 219 (1967).
- [12] See Supplemental Material at <http://link.aps.org/supplemental/10.1103/PhysRevLett.116.178301> for a detailed description of the numerical methods and analytical derivations, which contains Refs. [13–16].
- [13] P. Kloeden and E. Platen, *Numerical Solution of Stochastic Differential Equations* (Springer, Berlin, 1992).
- [14] R. E. Goldstein and S. A. Langer, *Phys. Rev. Lett.* **75**, 1094 (1995).
- [15] M. Hinczewski, X. Schlagberger, M. Rubinstein, O. Krichevsky, and R. R. Netz, *Macromolecules* **42**, 860 (2009).
- [16] C. Bennemann, J. Baschnagel, W. Paul, and K. Binder, *Comput. Theor. Polym. Sci.* **9**, 217 (1999).
- [17] G. Chirico and J. Langowski, *Biopolymers* **34**, 415 (1994).
- [18] H. Wada and R. R. Netz, *Europhys. Lett.* **77**, 68001 (2007).
- [19] J. K. G. Dhont, *An Introduction to Dynamics of Colloids* (Elsevier, Amsterdam, 1996).
- [20] X. Lu and Y. Hu, *Molecular Thermodynamics of Complex Systems* (Springer, Heidelberg, 2008).
- [21] T. Vicsek, A. Czirók, E. Ben-Jacob, I. Cohen, and O. Shochet, *Phys. Rev. Lett.* **75**, 1226 (1995).
- [22] I. H. Riedel, K. Kruse, and J. Howard, *Science* **309**, 300 (2005).
- [23] H. Chaté, F. Ginelli, G. Grégoire, and F. Raynaud, *Phys. Rev. E* **77**, 046113 (2008).
- [24] E. Bertin, M. Droz, and G. Grégoire, *Phys. Rev. E* **74**, 022101 (2006).
- [25] T. Ihle, *Phys. Rev. E* **83**, 030901 (2011).
- [26] F. Ginelli, F. Peruani, M. Bär, and H. Chaté, *Phys. Rev. Lett.* **104**, 184502 (2010).
- [27] F. Peruani, J. Starruß, V. Jakovljevic, L. Søgaard-Andersen, A. Deutsch, and M. Bär, *Phys. Rev. Lett.* **108**, 098102 (2012).
- [28] M. C. Marchetti, J. F. Joanny, S. Ramaswamy, T. B. Liverpool, J. Prost, M. Rao, and R. A. Simha, *Rev. Mod. Phys.* **85**, 1143 (2013).
- [29] Y. Yang, F. Qiu, and G. Gompper, *Phys. Rev. E* **89**, 012720 (2014).
- [30] A. Kaiser and H. Löwen, *Phys. Rev. E* **87**, 032712 (2013).
- [31] A. Peshkov, E. Bertin, F. Ginelli, and H. Chaté, *Eur. Phys. J. Spec. Top.* **223**, 1315 (2014).
- [32] E. Bertin, M. Droz, and G. Grégoire, *J. Phys. A* **42**, 445001 (2009).
- [33] A. Peshkov, I. S. Aranson, E. Bertin, H. Chaté, and F. Ginelli, *Phys. Rev. Lett.* **109**, 268701 (2012).
- [34] F. Thüroff, C. A. Weber, and E. Frey, *Phys. Rev. X* **4**, 041030 (2014).
- [35] C. A. Weber, F. Thüroff, and E. Frey, *New J. Phys.* **15**, 045014 (2013).
- [36] F. Thüroff, C. A. Weber, and E. Frey, *Phys. Rev. Lett.* **111**, 190601 (2013).
- [37] A. Peshkov, S. Ngo, E. Bertin, H. Chaté, and F. Ginelli, *Phys. Rev. Lett.* **109**, 098101 (2012).
- [38] J. Toner and Y. Tu, *Phys. Rev. Lett.* **75**, 4326 (1995).
- [39] A. Baskaran and M. C. Marchetti, *Phys. Rev. E* **77**, 011920 (2008).
- [40] S. Mishra, A. Baskaran, and M. C. Marchetti, *Phys. Rev. E* **81**, 061916 (2010).
- [41] I. S. Aranson and L. S. Tsimring, *Phys. Rev. E* **71**, 050901 (R) (2005).
- [42] I. S. Aranson and L. Kramer, *Rev. Mod. Phys.* **74**, 99 (2002).
- [43] V. García-Morales and K. Krischer, *Contemp. Phys.* **53**, 79 (2012).

- [44] L. Huber, J. Denk, E. Reithmann, E. Frey (to be published).
- [45] H. Chaté, F. Ginelli, G. Grégoire, F. Peruani, and F. Raynaud, *Eur. Phys. J. B* **64**, 451 (2008).
- [46] S. Fürthauer, M. Stempel, S. W. Grill, and F. Jülicher, *Eur. Phys. J. E* **35**, 89 (2012).
- [47] S. Fürthauer, M. Stempel, S. W. Grill, and F. Jülicher, *Phys. Rev. Lett.* **110**, 048103 (2013).
- [48] S. Ramaswamy, *Annu. Rev. Condens. Matter Phys.* **1**, 323 (2010).
- [49] H. H. Wensink, V. Kantsler, R. E. Goldstein, and J. Dunkel, *Phys. Rev. E* **89**, 010302 (2014).
- [50] K. H. Nagai, Y. Sumino, R. Montagne, I. S. Aranson, and H. Chaté, *Phys. Rev. Lett.* **114**, 168001 (2015).
- [51] J. Dunkel, S. Heidenreich, K. Drescher, H. H. Wensink, M. Bär, and R. E. Goldstein, *Phys. Rev. Lett.* **110**, 228102 (2013).
- [52] V. Bratanov, F. Jenko, and E. Frey, *Proc. Natl. Acad. Sci. U.S.A.* **112**, 15048 (2015).